ACS Catalysis

Research Article

pubs.acs.org/acscatalysis

Molecular Insight into Pt-Catalyzed Chemoselective Hydrogenation of an Aromatic Ketone by In Situ Modulation–Excitation IR Spectroscopy

Mengmeng Chen,[†] Nobutaka Maeda,[‡] Alfons Baiker,*[,‡,§] and Jun Huang*[,†]

[†]Laboratory for Catalysis Engineering, School of Chemical and Biomolecular Engineering, The University of Sydney, NSW 2006, Australia

[‡]Institute for Chemical and Bioengineering, Department of Chemistry and Applied Biosciences, ETH Zurich, Hönggerberg, HCl, CH-8093 Zurich, Switzerland

[§]Chemistry Department, Faculty of Science, King Abdulaziz University, P.O. Box 80203, Jeddah 21589, Saudi Arabia

Supporting Information

ABSTRACT: Chemoselective platinum-catalyzed liquid-phase hydrogenation of aromatic ketones is an important reaction in the production of fine chemicals and pharmaceuticals. A typical example of this class of reactions is the hydrogenation of acetophenone (AP) over a Pt/Al_2O_3 catalyst. We investigated the adsorption behavior of the different reaction components and their reaction pathways using in situ attenuated total reflection infrared spectroscopy in combination with modulation excitation spectroscopy and phase sensitive detection. AP adsorbed on both Pt and the alumina support. On Pt, AP adsorbed in the η^1 (O) configuration prevailed, whereas on alumina, AP bound to Lewis acid sites was predominant. In the presence of hydrogen, η^1 (O) AP adsorbed on Pt was hydrogenated to the main product, 1-phenylethanol (PE), with high selectivity (82.5%). The produced PE was more strongly adsorbed on the alumina support than on Pt, leading to replacement of AP and accumulation of PE on alumina. Co-adsorption experiments of AP with its products PE, 1-cyclohexylethanol, and ethylbenzene revealed that AP adsorbed in the η^1 (O) configuration was always the prevalent adsorption mode of AP on Pt, which may partly explain the high selectivity to PE observed. Co-adsorption of AP and CO did not significantly affect the adsorption of AP; however, CO adsorption strongly suppressed the adsorption and dissociation of H_2. The studies revealed a striking difference in the selectivity behavior between the gas-phase and liquid-phase hydrogenation. Although in the gas-phase hydrogenation of AP, a significant effect of decomposition/hydrogenolysis products on the chemoselectivity of AP hydrogenation was reported, these fragmentation reactions were barely observed in the liquid phase.

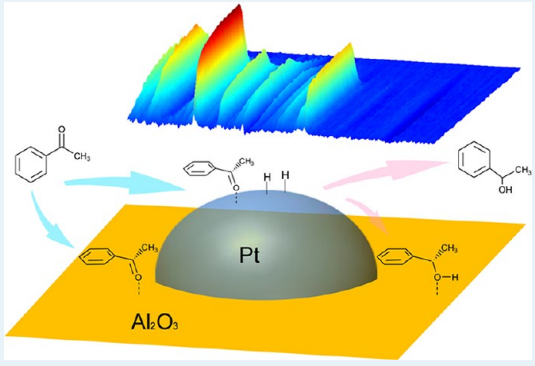

KEYWORDS: *chemoselective hydrogenation, acetophenone, aromatic ketones, Pt/Al_2O_3, liquid-phase, in situ attenuated total reflection infrared spectroscopy, modulation excitation spectroscopy, phase-sensitive detection*

1. INTRODUCTION

The chemoselective hydrogenation of unsaturated organic compounds containing carbonyl groups is of great importance not only in organic syntheses but also in bio-oil upgrading to fuels and high-value chemicals.[1−3] Particular attention is given to the chemoselective hydrogenation of aromatic ketones to the corresponding alcohols because of their role as intermediates in the pharmaceutical industries. Although some studies have been devoted to the reaction mechanism of the gas phase hydrogenation of aromatic ketones,[4−6] similar investigations in the liquid phase are scarce.[7−13]

Acetophenone (AP), as one of the simplest aromatic ketones, has received the most attention because it is an ideal model substrate containing the two typical functional groups, that is, the carbonyl moiety and aromatic ring. Competitive and consecutive hydrogenation of the carbonyl group and the aromatic ring give rise to a complex reaction network leading to several products and byproducts (Scheme 1).[5] The most desired reaction is that to 1-phenylethanol (PE) which is extensively used in perfumery products and pharmaceuticals.[14] AP hydrogenation has been widely studied in both the liquid and vapor phases over a variety of metal catalysts, including supported Pt, Pd, Ni, and Rh.[4,5,10,14−22] Although most of the existing reports focus on catalyst screening and optimization to improve catalytic properties in terms of their activity and selectivity.,[5,10,14−17,23,24] few studies have addressed the reaction kinetics and proposed mechanistic models.[18−22]

On the basis of in situ FT-IR spectroscopic study of the gas phase AP hydrogenation on Pt/SiO_2, Chen et al.[4] concluded that the selectivity of AP hydrogenation strongly depends on

Received: June 22, 2012
Revised: July 31, 2012
Published: August 1, 2012

Scheme 1. AP Hydrogenation Pathways

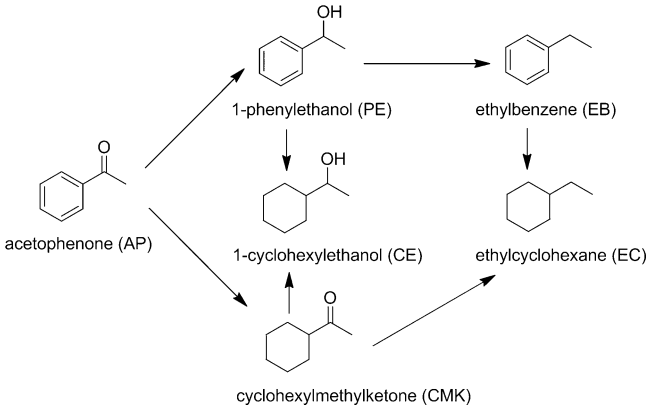

the formation of fragments (CO, benzene, toluene, and methane) originating from AP hydrogenolysis/decomposition and the strong adsorption of PE on the Pt surface. These fragments were supposed to inhibit the bonding between the phenyl group and Pt surface, leading to a decrease in the rate of the side reaction to 1-cyclohexylethanol (CE). Because most of the aromatic ketone hydrogenations are performed in the liquid-phase, the question arises whether this behavior is also true under liquid-phase conditions.

Attenuated total reflection infrared (ATR-IR) spectroscopy possesses several features that are excellently suited for in situ investigation of catalytic solid−liquid interfaces as encountered in heterogeneous catalysis.[25] It can provide information on the species adsorbed on the catalyst surface during reaction, such as intermediates, even in the presence of strongly absorbing solvents. In some cases, information about the catalyst itself can also be acquired. However, proper analysis of ATR-IR spectra of a multiphase system under working conditions is quite demanding because it simultaneously provides information about dissolved and adsorbed reactants and products, adsorbed intermediates, byproducts, and the catalyst itself.[26] To solve the difficulties of conventional ATR-IR in assigning absorption bands and analyzing kinetics, ATR-IR spectroscopy in combination with modulation excitation spectroscopy (MES) and phase sensitive detection (PSD) has gained increasing attention. The most favorable features of this technique are the enhanced signal-to-noise ratio (S/N ratio) and the discrimination between active and spectator species at catalytic solid−liquid interfaces.[27−29] Here, we used this technique to gain some molecular insight into the adsorption and reaction steps occurring during the platinum-catalyzed liquid-phase hydrogenation of AP.

2. EXPERIMENTAL SECTION

2.1. Materials. Acetophenone (Sigma-Aldrich, 99%), 1-phenylethanol (Sigma-Aldrich, 98%), 1-cyclohexylethanol (Sigma-Aldrich, 99%), ethylbenzene (Sigma-Aldrich, 99%), *n*-hexane (Sigma-Aldrich, 97%), ethanol (Sigma-Aldrich, 99.8%), and γ-Al_2O_3 (Umicore) were used as received. The commercial 5 wt % Pt/Al_2O_3 catalyst (BASF-Engelhard 4759) had a Pt dispersion of 0.27 and a BET surface area of 168 m^2/g. Prior to use, the catalyst was reduced in a fixed-bed reactor by first heating under helium flow from room temperature to 673 K; followed by reduction in pure hydrogen for 1 h at 673 K; cooling down in hydrogen for another 30 min; and finally, purging with helium flow for 30 min.

2.2. Preparation of Catalyst Layer and Infrared Spectroscopy. A thin film of pretreated catalyst was prepared for in situ IR measurements. A slurry of 90 mg of catalyst in 10 mL of ethanol was stirred overnight to achieve uniform suspension. Then, 1.6 mL of the slurry was brought onto a ZnSe internal reflection element (IRE, bevel of 45°, 52 mm × 20 mm × 2 mm, Crystran Ltd.), and after complete evaporation of ethanol, the film was placed in a home-built, stainless steel, flow-through cell.[30] The as-prepared catalyst layer adhered to the IRE so that no loss of catalyst was observed over the course of several hours under flow-through conditions. Prior to experiments, the Pt/Al_2O_3 layer was pretreated in situ by flowing hydrogen-saturated *n*-hexane for 3 h at 323 K. In situ IR experiments were performed in the flow-through cell, which was mounted onto an ATR-IR attachment (OPTISPEC). The temperature of the cell was controlled by a thermostat (Julabo, F25).

ATR-IR spectra were recorded on a Bruker IFS-66/S spectrometer equipped with a liquid-nitrogen-cooled MCT detector at 4 cm^{-1} resolution. Modulation−excitation spectroscopy was carried out by periodically changing between two different solutions: (i) AP (2 mM) in *n*-hexane and neat *n*-hexane solution; (ii) AP (2 mM) and PE (2 mM) in *n*-hexane and neat *n*-hexane; (iii) AP (2 mM) and CE (2 mM) in *n*-hexane and neat *n*-hexane; (iv) AP (2 mM) and EB (2 mM) in *n*-hexane and neat *n*-hexane. Corresponding solutions were fed from two separate glass-made bubble tanks in which the solutions can be saturated with gases such as He, H_2, and CO. The bubble tanks were connected to the flow-through cell via Teflon tubing. At the outlet, a peristaltic pump (ISMATEC, Reglo 100) was installed for continuously admitting solutions with a flow rate of 0.5 mL/min. Two interconnected pneumatically activated Teflon valves (Parker, PV-1−2324) were synchronized with the acquisition of IR spectra by spectrometer software (Bruker Optics, OPUS). Specifically, one cycle consisted of admission of substrate (2 mM) in *n*-hexane for 187.5 s or both substrate (2 mM) and product (2 mM) in *n*-hexane for 187.5 s, followed by subsequent admission of *n*-hexane for 187.5 s (total period of one cycle: 375 s). AP (saturated with He) concentration modulation was performed by admitting AP (2 mM) in *n*-hexane for 75 s, followed by admission of *n*-hexane for 75 s (total period of one cycle: 150 s). Typically, the experiments were carried out according to the following procedure: The initial three cycles were performed to obtain a stable response. Afterward, five cycles were repeated and averaged into one cycle to enhance the S/N ratio and time resolution. Phase-sensitive detection was used to further remove the noise and to obtain kinetic information of responding surface species. The phase-domain spectra were obtained by a mathematical treatment of the time-domain spectra according to the following equation:

$$A_k(\tilde{\nu})\cos(\varphi_k + \varphi_k^{\text{delay}}(\tilde{\nu})) = \frac{2}{T}\int_0^T A(t,\tilde{\nu})\sin(k\omega t + \varphi_k)\,dt \quad (1)$$

where T is the length of a cycle, ω is the demodulation frequency, φ_k is the demodulation phase angle, k is the demodulation index ($k = 1$ in this study), and $A(t,\tilde{\nu})$ and $A_k(\tilde{\nu})$ are the active species responses in the time and phase domains, respectively.

dx.doi.org/10.1021/cs300408x | ACS Catal. 2012, 2, 2007−2013

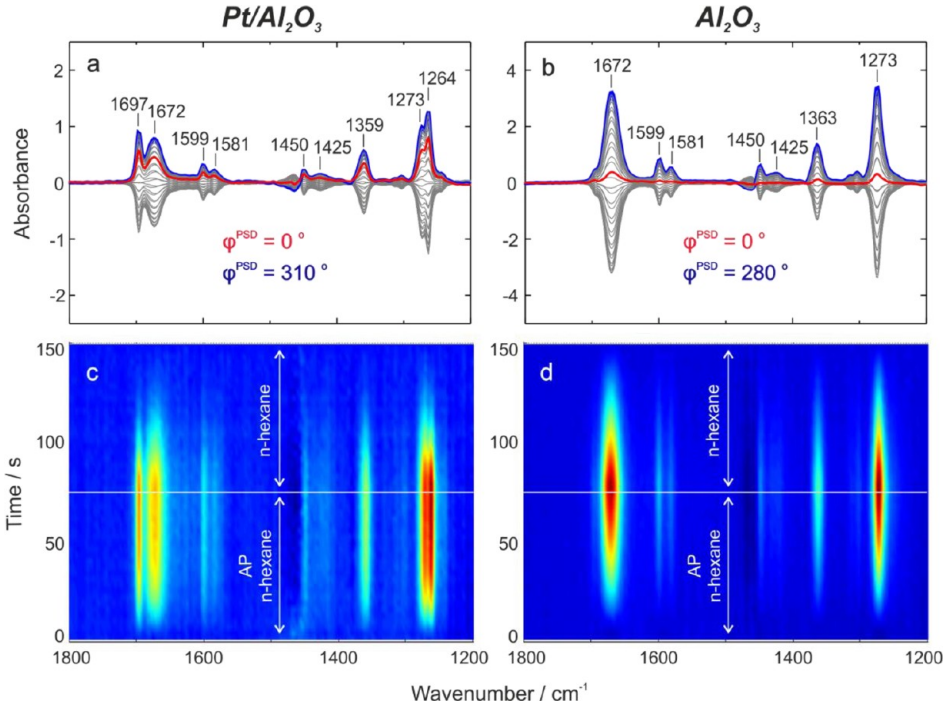

Figure 1. (a, b) Phase-domain and (c, d) time-domain ATR-IR spectra during adsorption and desorption of AP (2 mM) in He-saturated *n*-hexane on (a, c) Pt/Al_2O_3 and (b, d) Al_2O_3 at 298 K.

3. RESULTS AND DISCUSSION

3.1. Adsorption of Acetophenone (AP). In a first step, we used in situ ATR-IR in combination with MES and PSD to investigate AP adsorption−desorption in He-saturated *n*-hexane on Pt/Al_2O_3 and Al_2O_3 at 298 K. As shown in Figure 1a (phase-domain) and 1c (time-domain), splitting bands at 1697 and 1672 cm^{-1} were observed for the C═O stretching vibration (1682 cm^{-1} for the neat AP, as shown in Figure S1, in the Supporting Information) after AP adsorption on Pt/Al_2O_3. The band at 1672 cm^{-1} was identified as the C═O stretching vibration of AP adsorbed on Al_2O_3, as shown in Figure 1b and d, and the band at 1697 cm^{-1} can be assigned to the C═O stretching vibration of AP adsorbed on Pt (Figure 1a and c).

Similarly, the band at 1262 cm^{-1} attributed to X-sensitive benzene mode[31] of neat AP (Supporting Information Figure S1) was split into two bands at 1273 and 1264 cm^{-1}, respectively, in Figure 1a and c. Figure 1b and d indicates that the adsorption of AP on Al_2O_3 caused a shift of the X-sensitive benzene mode[31] of AP from 1262 to 1273 cm^{-1}. This C−C stretching vibration was shifted to 1264 cm^{-1} (Figure 1a and c) when AP adsorbed on Pt. Bands at 1359 cm^{-1} in Figure 1a and c and the band at 1363 cm^{-1} in Figure 1b and d are due to the bending mode of CH_3.[31,32] Bands at 1599, 1581, and 1450 cm^{-1} in Figure 1c and d were assigned to the C═C stretching vibrations of the phenyl group[4,31] and showed no band shift.

From the above findings, we conclude that AP adsorbed not only on Pt but also on the Al_2O_3 support. AP adsorption on Al_2O_3 most likely occurred via coordination to Lewis acid sites through one of the oxygen lone pairs, which might explain the significant red shift of the C═O stretching vibration (from 1682 cm^{-1} in the liquid phase to 1672 cm^{-1} on Al_2O_3).[33] On Pt, two adsorption configurations, η^1 (O) and η^2 (C, O), were proposed for AP adsorption.[4] According to Greenler's surface selection rule, any vibrational modes involving the dipole moment change parallel to the metal surface[34] cannot be observed. The dipole moment change of the η^2 (C, O) configuration should be canceled out; hence, the corresponding IR band disappears. Because the C═O band was clearly observable at 1697 cm^{-1}, AP was likely adsorbed on the Pt surface in the η^1 configuration.

Interestingly, the band intensity (1672 cm^{-1}) of the C═O stretching vibration of AP on Al_2O_3 (7.0 milliabsorbance) is much higher than that on Pt/Al_2O_3 (1.6 milliabsorbance). Moreover, the adsorption−desorption of AP was significantly slower on Al_2O_3 compared with that on Pt/Al_2O_3, as emerges from comparison of their phase-domain spectra presented in Figure 1a and b. In Figure 1a, the in-phase angle of absorption bands is φ = 310° with a phase delay of 50° (360−310°), whereas in Figure 1b, the in-phase angle of bands is φ = 280° with a phase-delay of 80° (360−280°).

3.2. Hydrogenation. When the solutions were saturated with H_2, the hydrogenation of AP started, and the reaction pathway was followed by in situ ATR-IR. As shown in Figure 2, new absorption bands at 1012, 1027, and 1081 cm^{-1} emerged due to C═C stretching, in-plane C−H bending, and C−O stretching vibration (υ(C−O) mode)[35] of the product (PE), which also gave rise to two other new bands at 1204 and 1494 cm^{-1} assigned to deformation of the phenyl ring[35] and phenyl C═C stretching vibration.[4] The slight blue shifts of 6 cm^{-1} for υ(C−O) of PE in the reaction compared with neat liquid phase PE (1075 cm^{-1}) were probably caused by its adsorption on the Al_2O_3 support.

Interestingly, the band at 1672 cm^{-1} of AP υ(C═O) adsorbed on the Al_2O_3 support quickly reached maximum intensity at 45 s and gradually decreased while the characteristic band of PE at 1081 cm^{-1} increased continuously. At the same time, the band at 1273 cm^{-1} of AP υ(C−C) on Al_2O_3 almost disappeared. However, the band intensity at 1697 and 1264 cm^{-1} due to υ(C═O) and the X-sensitive benzene mode of AP adsorbed on Pt still gradually increased with time until 187.5 s.

dx.doi.org/10.1021/cs300408x | ACS Catal. 2012, 2, 2007−2013

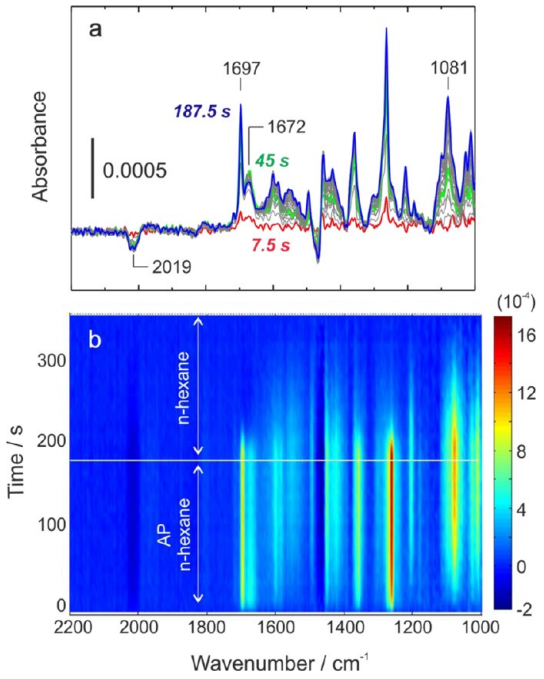

Figure 2. Time-domain ATR-IR spectra during hydrogenation of AP (2 mM) in H_2-saturated *n*-hexane on Pt/Al_2O_3 at 298 K.

The above observation suggests that PE originating from the selective hydrogenation of AP on Pt partially replaced AP preadsorbed on the Al_2O_3, indicating its stronger adsorption on the support. The AP desorbed from the support could either desorb to the bulk liquid phase or readsorb on Pt in the η^1 (O) configuration and undergo hydrogenation. This scenario is strikingly different from that proposed earlier for the gas-phase hydrogenation,[4] for which the strong adsorption and accumulation of PE on Pt were considered to be responsible for the high selectivity because of suppression of the formation of CE.[4]

The above in situ ATR-IR investigation shows that AP was adsorbed on Pt in its η^1 (O) mode, and PE was produced as a result of the favored hydrogenation of the carbonyl group. This behavior is also reflected in the results of experiments performed under the same conditions in a batch reactor (Table 1). PE was the dominant product, with a selectivity of 82.5%. Only a relatively small fraction of the AP probably underwent aromatic ring hydrogenation via π-bonded complex.[36]

Interestingly, the decomposition/hydrogenolysis of AP observed in the gas-phase hydrogenation that leads to various fragmentation products (CO, benzene, toluene, methane) is strongly suppressed in the liquid-phase hydrogenation. Only a small negative band appeared at 2019 cm^{-1}, which gradually decreased with increasing AP adsorption on Pt. Furthermore, this band was hardly discernible in the IR spectra, when products PE, CE, and EB were introduced into AP solution. Tentatively, we assign this band to low coverage of atop-bound CO on Pt steps, which is in the range of 2009−2030 cm^{-1}.[37] CO observed during the gas-phase hydrogenation of AP was attributed to the decomposition of η^2 (C, O) adsorbed AP on Pt.[4] In our liquid-phase experiments, no evidence for AP adsorbed in the η^2 (C, O) configuration could be found. Furthermore, no other decomposition products, such as benzene and toluene, were detected (see Table 1).

The above results indicate that decomposition of AP possibly occurred on only a few specific active sites at the beginning of the liquid-phase hydrogenation (no band at 2019 cm^{-1} during AP adsorption in Figure 1). During the whole hydrogenation process, AP η^1 (O) was dominant on Pt and is therefore assumed to be at the origin of the selective production of PE, as shown in Figure 2 and Table 1.

To gain further information about the influence of CO in this reaction network, CO was deliberately introduced during in situ IR investigations of AP hydrogenation. As shown in Figure 3, a positive band at 2074 cm^{-1} and a negative one at 2055 cm^{-1} due to CO linearly bound to Pt appeared in the IR spectrum. No band at 2019 cm^{-1} is discernible in Figure 3. This indicates that the band 2019 cm^{-1} in Figure 2 might stem from minor AP fragmentation on specific active sites. In addition, no competition between CO and AP adsorption on the catalyst surface was observed. Even in the presence of CO, AP could still strongly adsorb on the catalyst surface, as a comparison of the spectra in Figure 3 and Figure 1 reveals.

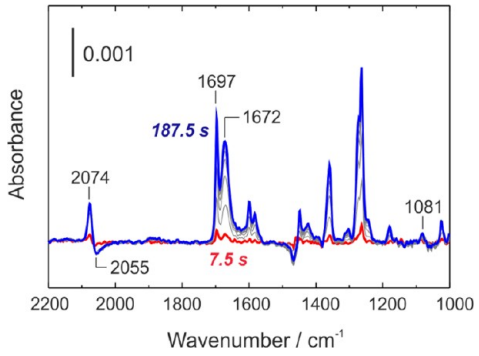

Figure 3. Time-domain ATR-IR spectra during hydrogenation of AP (2 mM) in H_2- and CO-saturated *n*-hexane on Pt/Al_2O_3 at 298 K.

However, AP hydrogenation was significantly inhibited in the presence of CO, because the characteristic absorption band of PE at 1081 cm^{-1} almost disappeared in Figure 3. Therefore, CO and H_2 were competitively adsorbed on the Pt sites, and CO completely blocked the adsorption of hydrogen on Pt for the further hydrogenation, whereas AP adsorption was barely affected by the presence of CO. The hydrogenolysis (decomposition) of AP on a few specific active sites likely occurred between AP η^2 (C, O) and nearby dissociated hydrogen. Without adsorbed H_2 in Figures 1 and 3, no CO band at 2019 cm^{-1} was detected from AP hydrogenolysis/decomposition. It seems that once CO covered these specific active sites, hydrogen adsorption was blocked, and no further decomposition of AP was detected (the negative band at 2019

Table 1. Acetophenone (AP) Hydrogenation[a]

	selectivity (%)					
reaction time	EC	EB	CMK	CE	PE	total conversion (%)
5 min	0	0	17.5	0	82.5	9.0
20 min	0	0	20.7	4.8	74.5	29.2
40 min	0	0	21.6	5.7	72.7	45.9
1 h	0	0	21.9	6.5	71.6	61.0

[a]Conditions: 20 mg of reduced Pt/Al_2O_3, 0.5 mmol of AP, 6 mL of *n*-hexane p_{H_2} = 1 bar, 298 K, magnetic stirring 500 rpm. Further details of autoclave experiments are given in the Supporting Information.

dx.doi.org/10.1021/cs300408x | ACS Catal. 2012, 2, 2007−2013

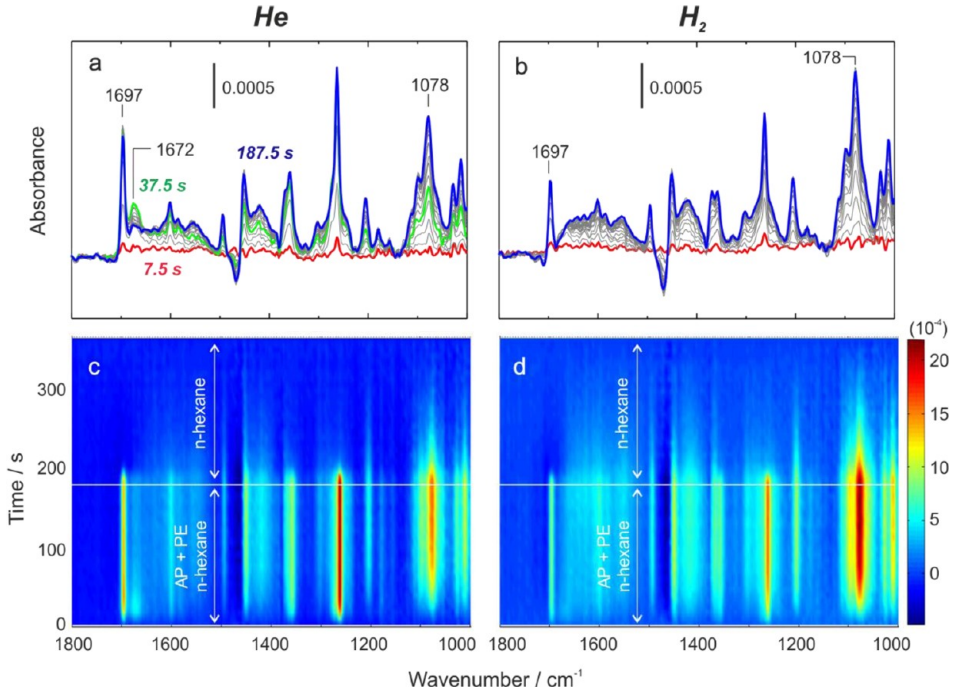

Figure 4. Time-domain ATR-IR spectra during adsorption and desorption of AP (2 mM) + PE (2 mM) in (a, c) He- and (b, d) H_2-saturated *n*-hexane on Pt/Al_2O_3 at 298 K.

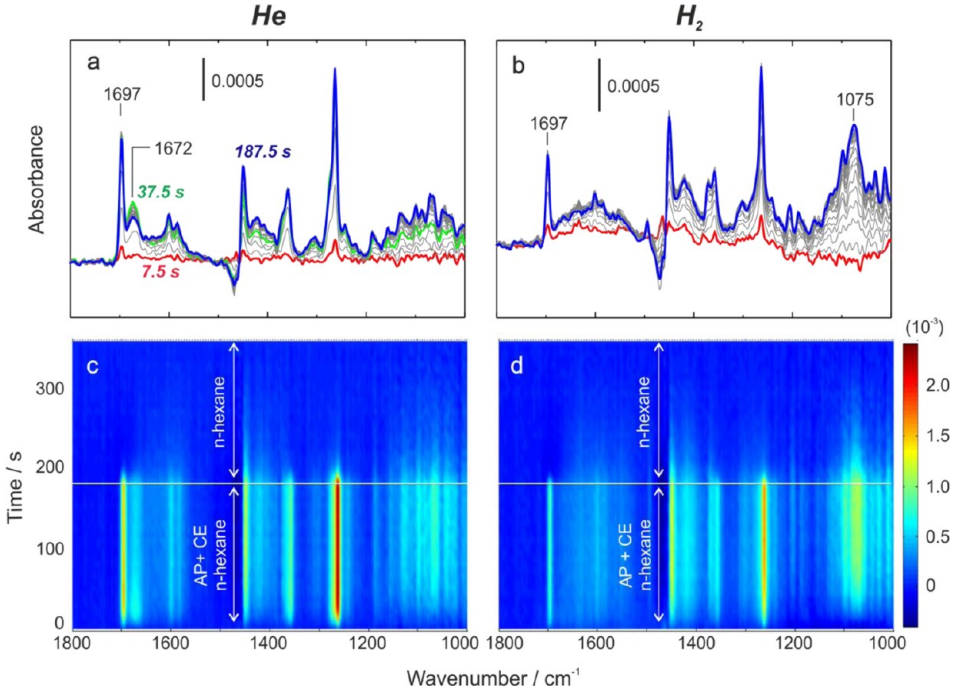

Figure 5. Time-domain ATR-IR spectra during adsorption and desorption of AP (2 mM) + CE (2 mM) in (a, c) He- and (b, d) H_2-saturated *n*-hexane on Pt/Al_2O_3 at 298 K.

cm^{-1}), as shown in Figure 2. Therefore, AP hydrogenolysis/decomposition as observed in the gas-phase reaction under vacuum conditions occurred only in the beginning of the liquid-phase hydrogenation and stopped because of blocking of these active sites by the fragmentation products.

3.3. Reaction Pathway. Scheme 1 shows the general reaction scheme previously proposed for the Pt-catalyzed AP hydrogenation. According to this scheme, AP hydrogenation can lead to four other products in addition to PE. Although CMK is only produced from AP, CE can be produced from either PE or CMK. EB is produced only from PE, but EC could be produced from EB and CE. To clarify the significance of the different reactions, coadsorption experiments of substrate and main products were carried out. Figure 4 shows ATR-IR spectra obtained by coadsorption of AP and PE saturated with either helium or hydrogen. As emerges from Figure 4a and c, upon admission of AP and PE in He-saturated *n*-hexane, the signals at 1264, 1273, 1358, 1585, and 1601 cm^{-1} belong to AP (Figure

dx.doi.org/10.1021/cs300408x | ACS Catal. 2012, 2, 2007−2013

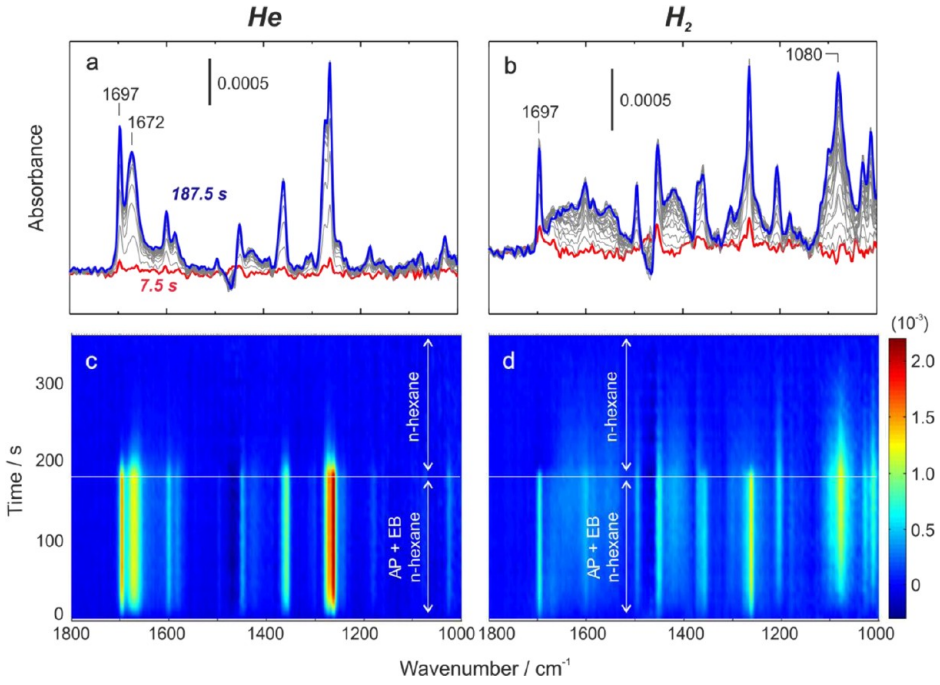

Figure 6. Time-domain ATR-IR spectra during adsorption and desorption of AP (2 mM) + EB (2 mM) in (a, c) He- and (b, d) H_2-saturated *n*-hexane on Pt/Al_2O_3 at 298 K.

1), and the bands at 1012, 1078, 1204, and 1494 cm^{-1}, which appeared on the same time scale, correspond to PE. AP preferentially adsorbed on the Pt surface via η^1 (O) (1697 cm^{-1}), and PE was largely adsorbed on the Al_2O_3 support (1078 cm^{-1}). Interestingly, the adsorption band at 1672 cm^{-1} quickly became saturated at 37.5 s and significantly decreased while the characteristic band at 1078 cm^{-1} grew. This phenomenon corroborated the observation made in Figure 2 that there was competitive adsorption of AP and PE on the Al_2O_3 support.

Upon replacing He- with H_2-saturated AP and PE in *n*-hexane, the adsorbed η^1 (O) AP was hydrogenated to PE. As shown in Figure 4b and d, the band at 1697 cm^{-1} of AP η^1 (O) on Pt decreased while the band at 1078 cm^{-1} of PE adsorbed on Al_2O_3 increased. During hydrogenation, the band at 1672 cm^{-1} of AP on Al_2O_3 almost disappeared as a result of the competitive adsorption of the newly produced PE. Apparently, the different adsorption properties of AP and PE significantly affected the processes occurring at the catalyst surface. For PE, no further reaction was detected because PE adsorbed on Al_2O_3 rather than on Pt. This is probably the reason that EB was hardly produced, even after AP hydrogenation in 1 h (Table 1).

The results shown in Figure 4 provide further evidence for the strikingly different behavior of the chemoselective hydrogenation of AP in the liquid and gas phases. It was proposed that in the gas phase, the selectivity of AP hydrogenation strongly depended on the fragmentation products (CO and benzene) from AP decomposition/hydrogenolysis and the strong adsorption of PE on Pt.[4] As emerges from Figure 4, in the liquid phase, PE adsorbed mainly on Al_2O_3 and less on Pt, and no significant band at 2019 cm^{-1} indicative of CO originating from AP fragmentation was discernible. Thus, it appears that fragmentation hardly occurs in the liquid phase, but it is significant in the gas-phase.

CE was not detected in the above IR investigation because it was not produced in the first few minutes during hydrogenation (see Table 1). However, with longer reaction times, formation of CE was significant, as shown in Table 1. To check whether the presence of CE affects AP hydrogenation, adsorption/desorption of AP and CE in He- and H_2-saturated *n*-hexane was studied (Figure 5). Upon admission of AP and CE in He (Figures 5a and c), bands at 1263, 1358, 1450, 1585, 1601, 1672, and 1697 cm^{-1} due to AP and bands in the range 1000−1200 cm^{-1} assigned to CE appeared. The bands of AP υ(C═O) on Al_2O_3 at 1672 cm^{-1} and η^1 (O) AP on Pt at 1697 cm^{-1} quickly reached maximum intensity at 37.5 s. With growing bands in the range 1000−1200 cm^{-1} (more adsorbed CE), the band at 1672 cm^{-1} (AP υ(C═O) on Al_2O_3) gradually decreased until 187.5 s, while the band at 1697 cm^{-1} (AP η^1 (O) on Pt) remained nearly at its maximum intensity from 37.5 to 187.5 s. This behavior corroborates that CE and AP competitively adsorbed on Al_2O_3, and the absorption of CE on Al_2O_3 was not as strong as that of PE.

Upon replacing H_2 with He in solvent (Figure 5b and d), the band of η^1 (O) AP on Pt at 1697 cm^{-1} decreased, while new bands appeared. The band at 1075 cm^{-1} due to PE υ(C−O) on the Al_2O_3 support gradually increased and overlapped with characteristic signals of CE in the region of 1000−1200 cm^{-1}. The band of AP υ(C═O) on Al_2O_3 at 1672 cm^{-1} disappeared, indicating that the PE that was formed replaced the AP on the support. The hydrogenation of AP to PE was hardly affected by the presence of CE, since CE apparently did not replace or block the AP η^1 (O) and hydrogen adsorption/dissociation on Pt.

At the beginning of the hydrogenation, CMK and PE were the only products, as shown in Table 1. CMK could be produced only through hydrogenation of the phenyl group of AP. To elucidate whether hydrogenation of the aromatic ring competed with the carbonyl group during AP hydrogenation, coadsorption and hydrogenation experiments of AP and EB were performed (Figure 6). During coadsorption of AP and EB in He-saturated *n*-hexane, characteristic bands of AP (1264,

dx.doi.org/10.1021/cs300408x | *ACS Catal.* 2012, 2, 2007−2013

1273, 1450, 1585, 1601, 1672, and 1697 cm^{-1}) appeared on the same time scale. Bands of AP υ(C═O) on Al_2O_3 and AP η^1 (O) on Pt (1672 and 1697 cm^{-1}) increased with time until 187.5 s, similar to that observed in the investigation without EB (Figure 1). AP adsorption on both Pt and Al_2O_3 via its carbonyl group consistently increased and was barely affected by EB.

Upon replacing He-saturated AP and EB with H_2-saturated AP and EB, new bands appeared at 1012, 1080, and 1204 cm^{-1} as a result of PE formation. The band at 1672 cm^{-1} assignable to υ(C═O) of AP on Al_2O_3 again significantly decreased because of the competitive adsorption of newly produced PE strongly adsorbed on Al_2O_3. The band at 1697 cm^{-1} corresponding to AP η^1 (O) on Pt hardly changed compared with the experiments without EB (Figure 2). Obviously, the presence of EB had only a minor effect on the adsorption behavior of AP.

5. CONCLUSION

In situ ATR-IR in combination with MES and PSD was applied to elucidate the surface processes occurring during the liquid-phase hydrogenation of AP on Pt/Al_2O_3. AP was predominantly adsorbed on Pt in its η^1 (O) configuration, and this species was hydrogenated with high chemoselectivity to PE. The produced PE was more strongly adsorbed on the Al_2O_3 support than on Pt, which may have led to enhanced desorption of PE from Pt. A smaller fraction of adsorbed AP probably also interacted with Pt via π-bonding of the aromatic ring, forming cyclohexylmethylketone (CMK). Co-adsorption experiments of AP with CO, PE, CE, and EB revealed that AP adsorbed in the η^1 (O) configuration was always the prevalent adsorption mode of AP on Pt. This behavior is strikingly different from that observed previously for AP hydrogenation in the gas phase, in which the fragmentation of AP by decomposition/hydrogenolysis and the strong adsorption of PE on Pt was reported to affect the chemoselectivity to PE.[4] Such behavior could not be observed in the liquid-phase, in which decomposition of AP played only a minor role in the beginning of the hydrogenation, indicated by the formation of some CO. Co-adsorption experiments of AP and CO showed that the presence of CO hardly affected the adsorption of AP, but significantly inhibited AP hydrogenation, since CO blocked H_2 adsorption and dissociation on the Pt surface.

■ ASSOCIATED CONTENT

Supporting Information

Experimental conditions of catalytic tests. IR spectra of liquid phase AP, PE, CE and EB. This material is available free of charge via the Internet at http://pubs.acs.org

■ AUTHOR INFORMATION

Corresponding Author

*E-mails: (A.B.) alfons.baiker@chem.ethz.ch, (J.H.) jun.huang@sydney.edu.au.

Notes

The authors declare no competing financial interest.

■ ACKNOWLEDGMENTS

This work was supported by the Early Career Research Scheme and the Major Equipment Scheme from the University of Sydney.

■ REFERENCES

(1) Huber, G. W.; Iborra, S.; Corma, A. *Chem. Rev.* **2006**, *106*, 4044.
(2) Mäki-Arvela, P.; Hájek, J.; Salmi, T.; Murzin, D. Y. *Appl. Catal., A* **2005**, *292*, 1.
(3) Nishimura, S. *Handbook of Heterogeneous Catalytic Hydrogenation for Organic Synthesis*; John Wiley & Sons: New York, 2001.
(4) Chen, C.-S.; Chen, H.-W.; Cheng, W.-H. *Appl. Catal., A* **2003**, *248*, 117.
(5) Chen, C.-S.; Chen, H.-W. *Appl. Catal., A* **2004**, *260*, 207.
(6) Chen, C.-S.; Chen, H.-W. *J. Chem. Soc., Faraday Trans.* **1996**, *92*, 1595.
(7) Bonnier, J. M.; Court, J.; Wierzchowski, P. T.; Hamar-Thibault, S. *Appl. Catal.* **1989**, *53*, 217.
(8) Kumbhar, P. S. *Appl. Catal., A* **1993**, *96*, 241.
(9) Santori, G. F.; Moglioni, A. G.; Vetere, V.; Iglesias, G. Y. M.; Casella, M. L.; Ferretti, O. A. *Appl. Catal., A* **2004**, *269*, 215.
(10) Drelinkiewicza, A.; Waksmundzka, A.; Makowski, W.; Sobczak, J. W.; Król, A.; Zieba, A. *Catal. Lett.* **2004**, *94*, 143.
(11) Hoxha, F.; Schmidt, E.; Mallat, T.; Schimmoeller, B.; Pratsinis, S. E.; Baiker, A. *J. Catal.* **2011**, *278*, 94.
(12) Hoxha, F.; Schimmoeller, B.; Cakl, Z.; Urakawa, A.; Mallat, T.; Pratsinis, S. E.; Baiker, A. *J. Catal.* **2010**, *271*, 115.
(13) Schimmoeller, B.; Hoxha, F.; Mallat, T.; Krumeich, F.; Pratsinis, S. E.; Baiker, A. *Appl. Catal., A* **2010**, *374*, 48.
(14) Huang, J.; Jiang, Y.; van Vegten, N.; Hunger, M.; Baiker, A. *J. Catal.* **2011**, *281*, 352.
(15) Jutz, F.; Andanson, J.-M.; Baiker, A. *J. Catal.* **2009**, *268*, 356.
(16) Malyala, R. V.; Rode, C. V.; Arai, M.; Hegde, S. G.; Chaudhari, R. V. *Appl. Catal., A* **2000**, *193*, 71.
(17) Lin, S. D.; Sanders, D. K.; Albert Vannice, M. *Appl. Catal., A* **1994**, *113*, 59.
(18) Rajashekharam, M. V.; Bergault, I.; Fouilloux, P.; Schweich, D.; Delmas, H.; Chaudhari, R. V. *Catal. Today* **1999**, *48*, 83.
(19) Gao, F.; Allian, A. D.; Zhang, H.; Cheng, S.; Garland, M. *J. Catal.* **2006**, *241*, 189.
(20) Bergault, I.; Rajashekharam, M. V.; Chaudhari, R. V.; Schweich, D.; Delmas, H. *Chem. Eng. Sci.* **1997**, *52*, 4033.
(21) Bergault, I.; Fouilloux, P.; Joly-Vuillemin, C.; Delmas, H. *J. Catal.* **1998**, *175*, 328.
(22) Bergault, I.; Joly-Vuillemin, C.; Fouilloux, P.; Delmas, H. *Catal. Today* **1999**, *48*, 161.
(23) Huck, W.-R.; Mallat, T.; Baiker, A. *Adv. Synth. Catal.* **2003**, *345*, 255.
(24) Schmidt, E.; Vargas, A.; Mallat, T.; Baiker, A. *J. Am. Chem. Soc.* **2009**, *131*, 12358.
(25) Andanson, J.-M.; Baiker, A. *Chem. Soc. Rev.* **2010**, *39*, 4571.
(26) Bürgi, T.; Baiker, A. *Adv. Catal.* **2006**, *50*, 227.
(27) Bürgi, T.; Baiker, A. *J. Phys. Chem. B* **2002**, *106*, 10649.
(28) Maeda, N.; Hungerbühler, K.; Baiker, A. *J. Am. Chem. Soc.* **2011**, *133*, 19567.
(29) Maeda, N.; Sano, S.; Mallat, T.; Hungerbühler, K.; Baiker, A. *J. Phys. Chem. C* **2012**, *116*, 4182.
(30) Urakawa, A.; Wirz, R.; Bürgi, T.; Baiker, A. *J. Phys. Chem. B* **2003**, *107*, 13061.
(31) Gambi, A.; Giorgianni, S.; Passerini, A.; Visinoni, R.; Ghersetti, S. *Spectrochim. Acta, Part A* **1980**, *36*, 871.
(32) Huang, H. G.; Huang, J. Y.; Cai, Y. H.; Xu, G. Q. *Chem. Phys. Lett.* **2005**, *414*, 143.
(33) Raskó, J.; Kiss, J. *Appl. Catal., A* **2005**, *287*, 252.
(34) Greenler, R. G. *J. Chem. Phys.* **1996**, *44*, 310.
(35) Shin-ya, K.; Sugeta, H.; Shin, S.; Hamada, Y.; Katsumoto, Y.; Ohno, K. *J. Phys. Chem. A* **2007**, *111*, 8598.
(36) Basset, J. M.; Dalmai-Imelik, G.; Primet, M.; Mutin, R. *J. Catal.* **1975**, *37*, 22.
(37) Lebedeva, N. P.; Rodes, A.; Feliu, J. M.; Koper, M. T. M.; van Santen, R. A. *J. Phys. Chem. B* **2002**, *106*, 9863.